LA-UR- 97-1168

Title: **PERFORMANCE OF ANALYTICAL METHODS FOR TOMOGRAPHIC GAMMA SCANNING**

Author(s): **T. H. Prettyman and D. J. Mercer**

Submitted to: **OSS Milestone**
FOR GENERAL DISTRIBUTION

MASTER

(PROGRESS REPORT)

AH

DISTRIBUTION OF THIS DOCUMENT IS UNLIMITED

Los Alamos
NATIONAL LABORATORY

Form No. 836 R5
ST 2629 10/91

DISCLAIMER

Performance of Analytical Methods for Tomographic Gamma Scanning

T. H. Prettyman and D. J. Mercer

Abstract

The use of gamma-ray computerized tomography for nondestructive assay of radioactive materials has lead to the development of specialized analytical methods. Over the past few years, Los Alamos has developed and implemented a computer code, called ARC-TGS, for the analysis of data obtained by tomographic gamma scanning (TGS). ARC-TGS reduces TGS transmission and emission tomographic data, providing the user with images of the sample contents, the activity or mass of selected radionuclides, and an estimate of the uncertainty in the measured quantities. The results provided by ARC-TGS can be corrected for self-attenuation when the isotope of interest emits more than one gamma-ray. In addition, ARC-TGS provides information needed to estimate TGS quantification limits and to estimate the scan time needed to screen for small amounts of radioactivity. In this report, an overview of the analytical methods used by ARC-TGS is presented along with an assessment of the performance of these methods for TGS.

Funding Statement

This work was funded by the Department of Energy, Office of Safeguards and Security

for general distribution

Introduction

Tomographic Gamma Scanning (TGS) is a gamma-ray nondestructive assay (NDA) technique developed by the Los Alamos Safeguards Program to accurately assay special nuclear material (SNM) in heterogeneous samples, particularly residues and waste, in large and small containers. TGS uses transmission tomography to form three-dimensional images of the linear attenuation coefficient for each sample. An isotopic transmission source that emits more than one gamma-ray, typically Se-75, is used to obtain attenuation images as a function of energy. The spatial distribution of gamma-ray emitting material is determined by emission tomography. High resolution gamma-ray spectroscopy (HRGS) is used to enable accurate measurements of the intensity of gamma-rays in complex spectra. The emission images are corrected for the attenuation of gamma-rays by the matrix using the linear attenuation coefficient images obtained by transmission tomography. The amount of radioactivity in a region-of-interest can be determined by integrating the emission image over the volume of the region.

Assays obtained by TGS are insensitive to the matrix and the location of gamma-ray emitting material. Consequently, TGS is the first truly general NDA method and, as such, can be applied to accurately assay any sample, provided the following conditions are met:

1. the sample is not completely opaque to the emitted gamma-rays,

2. the gamma-ray emitted by the isotope of interest is detectable, and
3. the gamma-ray emitted by the isotope of interest is not interfered with by other gamma-rays.

Analysis of TGS data is accomplished using the ARC-TGS computer code. ARC-TGS consists of Fortran 77 subroutines and programs that perform different functions needed to analyze TGS data. These routines have been used to analyze all of the data obtained by the prototype and mobile TGS systems. The data set consists of laboratory test samples with known matrix and SNM content (both plutonium and uranium), plutonium residues (e.g. from Rocky Flats and the Los Alamos Plutonium Facility), and transuranic waste from the Los Alamos waste storage facilities. Several hundred samples have been analyzed. The data and results for a subset of these samples have been archived for quality assurance and to enable the performance of enhancements to ARC-TGS to be evaluated.

ARC-TGS is currently implemented on Unix workstations. Coordination of the acquisition of TGS data on a PC and the analysis of the data on the workstation is accomplished using a file-based message protocol. Specific analysis tasks are accomplished using Unix shell scripts. Currently, we are using custom 300 MHz DEC Alpha computers from Microway ("Screamers"). These computers are inexpensive and provide the computational power needed to achieve throughput requirements for research and development.

Some of the ARC-TGS routines, particularly those that are time-intensive, can be executed in parallel on a workstation cluster. Parallel processing is currently accomplished using Parallel Virtual Machine (PVM), developed by Oak Ridge National Laboratory. A version of PVM is now available for Windows/NT. In addition, over the next year, the computing power of personal computers (PCs), particularly the Intel P7 architecture, is expected to improve significantly over the next year. Consequently, ARC-TGS could be implemented on a PC in the near future with little or no throughput penalty.

ARC-TGS provides three basic functions necessary for nondestructive assay using gamma-ray computerized tomography:

1. preprocessing and reconstruction of transmission data,
2. reconstruction of emission images, corrected for attenuation,
3. estimation of the mass of selected isotopes and an analysis of the uncertainty.

ARC-TGS provides information needed to accomplish additional tasks, including self-attenuation correction and sensitivity estimates. In this report, we will provide an overview of each of the basic functions and an assessment of the performance of ARC-TGS for TGS analysis.

Scanning Protocol and Data

The scanning protocol implemented in first-generation TGS instruments involves translating and rotating the sample at constant speed. While in motion, the elevation of the sample is fixed. So, to obtain complete coverage of the sample, the scan must be

repeated at different elevations. While in motion, spectrum region-of-interest (ROI) counts are downloaded from the gamma-ray spectrometer's analog-to-digital (ADC) converter to the data acquisition computer and stored in memory. ROI counts are acquired for fixed true-time intervals and a reference source (usually Cd-109) is used to provide a live-time estimate. Three ROIs are usually established for each full-energy peak: two ROIs for estimating the continuum level (one above the peak and one below); and a single ROI containing the peak to estimate gross counts. Net counts in a peak can be estimated, for example, for symmetric background ROIs by

$$N = (G - cB) \cdot CF(RL) \qquad \text{Eq. 1}$$

where G is counts in the peak ROI, B is the sum of counts in the background ROI, and c is the ratio of the number of channels in the peak ROI to the number of channels in the background ROIs. The correction factor for rate-loss ($CF(RL)$) is typically obtained by a "live-time" source, a source that injects a fixed rate of gamma-ray full-energy events into the detector.

Each measurement (sets of ROI counts for different gamma-rays) can be related to a discrete displacement (s) and angle of rotation (θ). For example, the locus of points in s,θ space for a low-resolution TGS scan is given in Figure 1 along with the scanner geometry. Note that there are a total of 150 discrete measurements. The sample is rotated 10 times during the scan and the direction of translation is reversed half-way through. The range of s,θ values covered in the scan is sufficient for tomographic reconstruction; however, the sampling of s,θ space is unusual and requires special consideration. The low-resolution scanning protocol provides enough information to reconstruct an image with 10x10x16 volume elements.

Typically, the counting interval for each measurement selected to be 6/10 sec. So, the scan at each elevation is completed in 90 seconds. The number of discrete elevations needed depends on the aspect-ratio of the sample. For 208-L drums, 16 elevations are sufficient and a complete, 1-pass scan can be completed in 24 minutes.

Higher resolution scans are also implemented for special applications, including scans corresponding to images 20x20x32 and 40x40x64 in size. For fixed contrast, the throughput of these scans is reduced. For example, the scan time required for the 20x20x32 scan is 8 times that of the 10x10x16 scan. In practice, the counting interval is usually reduced to maintain constant throughput.

The short count times encountered in these situations provide challenges to the data acquisition system and the analytical methods used to reduce the data. For example, HRGS electronics are usually designed to provide accurate results for long count times (> 1 minute). With TGS, count times can drop below 0.1 s. We have observed that transistor-reset preamplifiers, commonly used for high count rate applications, can stop functioning for over 1 s at a time. During that interval, no counts are registered and, depending on the counting interval, as many as 10 measurements can be "lost." The rate at which data is lost depends on the gross count rate. For transmission measurements,

where the gross input rate can exceed 300,000 counts per second, it is not uncommon to observe such an event once or twice in a complete scan (several lost measurements out of 150x16). The problem can be eliminated by switching to a resistive-feedback preamplifier with some loss of dynamic range.

In general, the developer of TGS analysis methods must be prepared to reconstruct images and to estimate the amount of radioactivity in the sample from incomplete data. The incompleteness of the data stems not only from limitations of the counting electronics, but also from the range and variety of samples that are encountered in practice. Waste and residue matrix material is highly variable in density and composition (e.g., ranging from low-density paper to high-density cement). For samples with dense inclusions, portions of the transmission data set have low counts and are, in effect, missing. To avoid indeterminate solutions, computer codes that analyze TGS data must be sophisticated enough to recognize this situation and to accurately estimate the linear-attenuation coefficient of the dense region.

In addition, to being incomplete, TGS data is non-ideal. When computerized tomography is applied to medical and industrial applications, the scanner hardware is usually designed so that the geometry of each measurement is nearly a line (or "ray"). This can be accomplished because such systems do not require HRGS. A large number of small detectors along with a high-intensity source are used to maximize throughput. With ray-geometry and high count rates, there are a number of well-known algorithms to reduce high resolution data sets (1024x1024) at high speed (e.g. filtered back-projection (FBP)).

Such algorithms are of limited use for TGS. First-generation scanners use a single intrinsic germanium detector. This is done to minimize the cost and complexity of the system and to remain consistent with existing gamma-ray assay technology. In order to achieve the desired throughput (at least one sample per hour), the scanner is usually operated in a low-resolution mode. The geometry of the measurements departs significantly from the ideal ray, particularly for emission measurements. The exact geometry of the measurement must be modeled in order to get accurate results. The unusual sampling of s,θ space also limits the application of direct reconstruction technique (such as FBP) to TGS analysis.

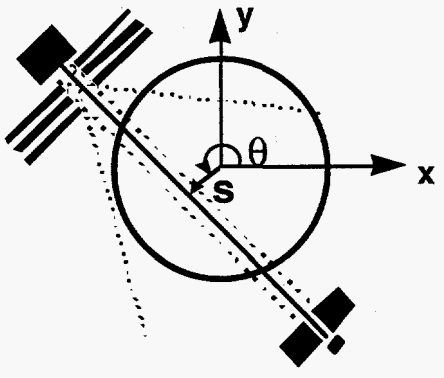

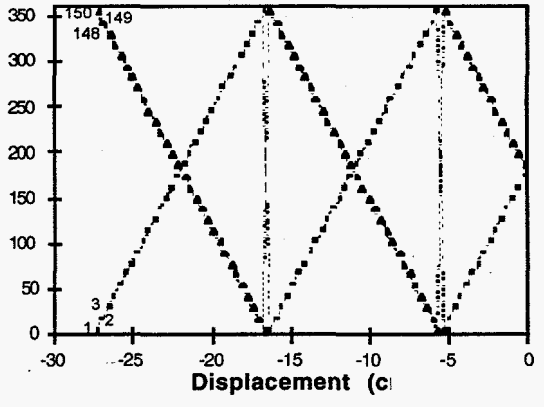

Figure 1. Geometry of a first-generation TGS scanner and the locus of points in displacement-angle space generated in a first-generation scan.

Transmission Analysis

The objective of the transmission analysis is to determine the linear attenuation coefficient (μ) of the sample as a function of position (x,y,z) and energy (E). To accomplish this, the sample is scanned with the source shutter open allowing a collimated beam of gamma-rays to pass through the sample. The transmission source is usually Se-75 which has three useful gamma-rays (136-keV, 280-keV, and 401-keV). For measurements of dense objects, however, it is not uncommon to use a high-energy source such as Co-60 along with Se-75. For our applications, the activity of the source can range from 20 mCi to 200 mCi.

The transmission data set consists of ROI counts for each gamma-ray emitted by the transmission source ($G_{k,l}$,c_k,$B_{k,l}$) and ROI counts for a reference gamma-ray emitted by a "live-time" source ($G_{R,l}$,c_R,$B_{R,l}$), where k and l are the energy and measurement indices, respectively. The transmission can be estimated by

$$T_{k,l} = \left(\frac{N_{k,l}}{N_{R,l}}\right) \Big/ \left(\frac{N_{k,ST}}{N_{R,ST}}\right) \qquad \text{Eq. 2}$$

where the net counts N are given by Equation 1. $N_{k,ST}$ and $N_{R,ST}$ are the net counts obtained for a transmission measurement obtained without the sample present. The opacity of the sample (the product of linear attenuation coefficient and length) can be estimated by:

$$O_{k,l} = -\ln\left(T_{k,l}\right) \qquad \text{Eq. 3}$$

An accurate model of the transmission in terms of the measurement geometry and sample matrix is given by:

$$T(s,\theta,E) = \int_{(S_l,\Theta_l)} ds'd\theta' \; w(s'-s,\theta'-\theta,E)\exp\left(-o(s',\theta',E)\right) \qquad \text{Eq. 4}$$

where (S_l, Θ_l) denotes set of rays connecting the source and the detector and $w(\delta s, \delta\theta, E)$ is a weighting function that includes, for example, angular variations in the detector efficiency. For the purpose of discussion, Eq. 4 considers two spatial dimensions, but in practice, the paths that gamma-rays take through the object are modeled in three-dimensions. The "opacity" of the sample is given by a line integral known in the vernacular of computerized tomography as a "ray-sum":

$$o(s,\theta,E)=\int_{-\infty}^{\infty}dx\int_{-\infty}^{\infty}dy\;\mu(x,y,E)\,\delta(x\cos\theta+y\sin\theta-s) \quad \text{Eq. 5}$$

For the purposes of reconstruction, the spatial and energy dependence of linear attenuation must be represented by a finite number of parameters. Discretization of the above equations is accomplished by first representing the linear attenuation coefficient as the sum of basis functions (the "series-expansion" method):

$$\mu(x,y,E)=\sum_i \mu_i(E)B_i(x,y) \quad \text{Eq. 6}$$

Substitution of Equation 5 into Equation 4 leads to the familiar algebraic expression:

$$o(s,\theta,E)=\sum_i C_i(s,\theta)\mu_i(E) \quad \text{Eq. 7}$$

where

$$C_i(s,\theta)=\int_{-\infty}^{\infty}dx\int_{-\infty}^{\infty}dy\;B_i(x,y)\,\delta(x\cos\theta+y\sin\theta-s) \quad \text{Eq. 8}$$

is just the Radon transform of the basis function. It is usually, but not always the case that the basis function is invariant under translation (e.g. as with pixels). So, the Radon transform can be computed once and stored for later use, resulting in a significant savings in compute time.

An example of the application of basis functions other than pixels to transmission computerized tomography is illustrated in Figure 2, in which transmission tomographs formed using two different image models are compared. With pixels, it is assumed that the sample is uniform over square or rectangular regions. With low-resolution tomography, pixels produce images that are blocky and features in the sample are not well resolved. Non-square image elements are possible. In addition the assumption of uniformity can also be relaxed. For example, images obtained from the same data set using tent-shaped local basis functions are shown in Figure 2. The tent-functions are two-dimensional and overlap one another. The same number of parameters are needed to represent an image with pixels and tent functions. However, the images obtained using tent-functions have higher contrast and resolution than the images obtained using pixels Most significantly, assays obtained using tent-functions to represent the attenuation image are more accurate than those obtained using pixels (see Figure 3). This illustrates the importance of the selection of image models for quantitative, low-resolution tomography.

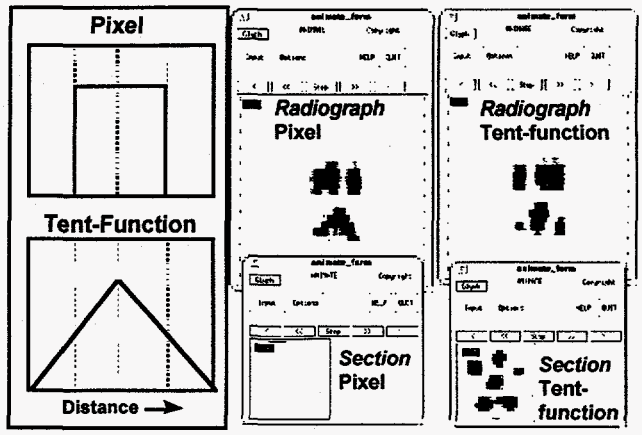

Figure 2. Comparison between transmission tomographs formed using two different image models (pixels and tent-shaped local basis functions).

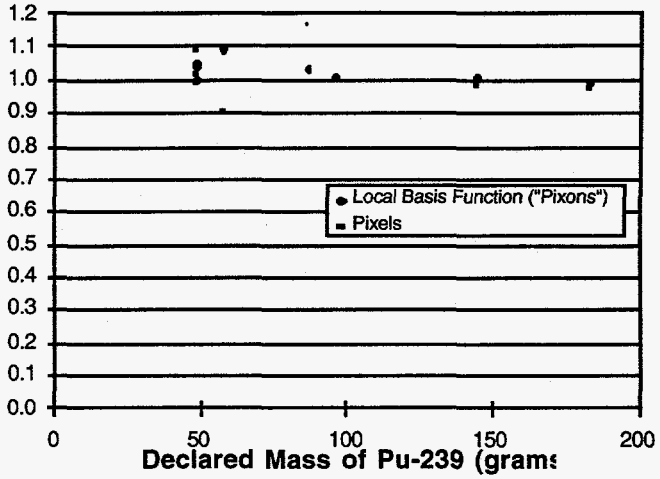

Figure 3. Comparison between assays using pixels and tent-shaped local-basis-functions in the transmission analysis.

To complete the discussion on discretization of the transmission equations, we must consider how to represent the dependence of the linear attenuation coefficient on energy. The linear attenuation coefficient can be accurately represented by an effective composition (n,Z), where n is the local electron density and Z is atomic number. We use a function of the following form:

$$\mu_i(E) = n_i \sum_p s_p(Z_i, E) \qquad \text{Eq. 9}$$

where the functions s_p model the dependence of the photoelectric effect and pair-production on atomic number. This is the most compact and accurate representation of the attenuation coefficient when the composition of the sample is unknown.

The transmission model given by Eqs. 4-9 is complete, accurate, and compact, involving just two images, n_i and Z_i. In principle, the model could fitted directly to the

measured transmission data, for example, using nonlinear least squares or maximum likelihood analysis. Due to the scale of the problem, this is not practical. Fortunately, there is a more direct way to obtain the desired result.

The main problem is that the ray-sums for each measurement are involved in a nonlinear expression that is time-consuming to evaluate (Eq. 4). A well-known solution to this problem is to replace Eq. 4 by the following:

$$T(s,\theta,E) = \exp\left(-O(s,\theta,E)\right)$$

$$O(s,\theta,E) = \int_{(S,\Theta_t)} ds'd\theta' \; \hat{w}(s'-s,\theta'-\theta,E)\, o(s',\theta',E) \qquad \text{Eq. 10-11}$$

where O is the expectation of the measured opacity and $\hat{w}(\delta s,\delta\theta,E)$ is an approximate weighting function. Eqs. 10-11, while an approximation, enable measurements with finite geometry to be modeled with reasonable accuracy. Eq. 4 is used only when the composition of portions of the sample are known (e.g. to model the container walls). Using Eqs. 7 and 8, Eq. 11 can be reduced to an expression that is linear in terms of the attenuation coefficient:

$$O(s,\theta,E) = \sum_i \hat{C}_i(s,\theta)\mu_i(E) \qquad \text{Eq. 12}$$

where

$$\hat{C}_i(s,\theta) = \sum_i \int_{(S,\Theta)} ds'd\theta' \; w(s'-s,\theta'-\theta,E)\; C_i(s,\theta) \qquad \text{Eq. 13}$$

With the approximate model, the amount of time required to evaluate the transmission is reduced considerably. In principle, the measured transmission could be converted to opacity directly via the log-transform and the linear attenuation coefficient image for each transmission source energy could be determined by solving a linear system. In this way, an attenuation coefficient image could be formed for each transmission source energy. The variation of the attenuation coefficient with energy could be determined for each pixel (or voxel) by fitting n and Z to the attenuation data using Equation 9.

Unfortunately, this approach is not very attractive for practical applications. The main problem is that when the data set is noisy, the problem cannot be de-coupled. Eqs. 9 and 12 must be solved simultaneously in order to obtain a solution. This limits the scale of the problem that can be solved.

A better approach is to represent the *opacity* in terms of an effective composition:

$$O_l(E) = N_l \sum_p s_p(Z_l,E) \qquad \text{Eq. 14}$$

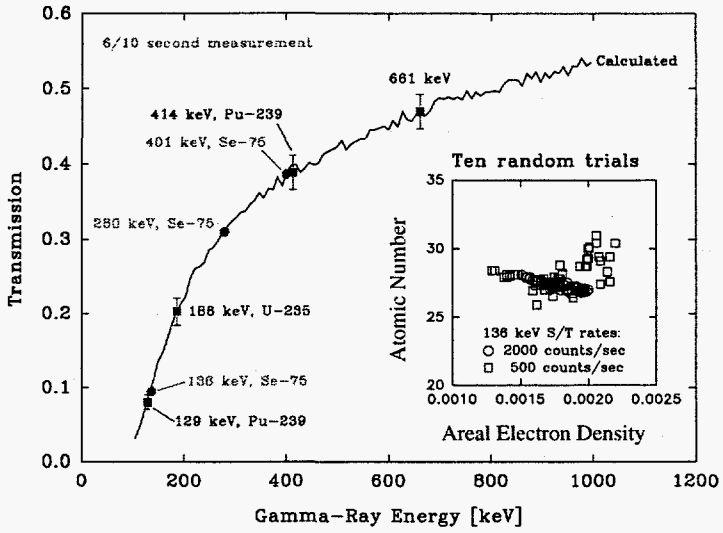

Figure 4. Interpolation and extrapolation of transmission measurements using a two-parameter, effective-composition model.

used in the simulations was 6/10 s. Two different source intensities were simulated. Eq. 14 was fitted to the transmission data obtained for each measurement. The fitted areal electron density and atomic number were used to estimate the transmission at four common gamma-ray energies (129-,186-,414-, and 661-keV). Transmissions obtained using the model at the four selected energies matched the calculated transmission to within the standard deviation of the population.

The two possible approaches that we have described for calculating attenuation coefficients as a function of energy are outlined in Table 1. With image-domain interpolation, the parameters needed to fit the attenuation coefficient for each pixel (or voxel) are determined from images reconstructed directly from the measured transmission. With projection-domain interpolation, the energy-variation of the attenuation coefficient determined for selected energies by reconstruction of interpolated transmissions. The image-domain and projection-domain approaches are equivalent in terms of accuracy. However, the projection-domain algorithm offers some advantages over the image-domain approach when large statistical variations in the transmission counting data are encountered.

With projection-domain interpolation, the energy-variation of the attenuation coefficient determined for selected energies by reconstruction of interpolated transmissions. The image-domain and projection-domain approaches are equivalent in terms of accuracy. However, the projection-domain algorithm offers some advantages over the image-domain approach when large statistical variations in the transmission counting data are encountered.

measure $T_{k,l}$

compute $O_{k,l} = -\ln\left(T_{k,l}\right)$

Image-domain interpolation	**Projection-domain interpolation**
Reconstruct $\mu_i(E_k)$ **by solving**	**Fit** N_i **and** Z_i **to the transmission data**
$O_{k,l} = \sum_i \hat{C}_i(s_l,\theta_l)\mu_i(E_k)$	**Compute** $O_l(E)$ **for a selected energy using**
Fit n_i **and** Z_i **to the attenuation image data**	$O_l(E) = N_l \sum_p s_p(Z_i, E)$
Compute $\mu_i(E)$ **for a selected energy using**	**Reconstruct** $\mu_i(E)$ **by solving**
$\mu_i(E) = n_i \sum_p s_p(Z_i, E)$	$O_l(E) = \sum_i \hat{C}_i(s_l,\theta_l)\mu_i(E)$

Table 1. Two methods for estimating linear attenuation coefficient images as a function of energy.

Samples with dense inclusions are often encountered in waste and residue assay. The dynamic range of transmission measurements made by TGS is limited. An isotopic source is used and the count time per measurement is short. The statistical variation in the measured transmission can be quite large when dense materials are encountered and the estimated amount of radioactive material within dense regions can be biased considerably because the attenuation coefficient is not know precisely. In the worst case, the assay can be indeterminate because the statistical quality of the transmission data was insufficient to estimate the attenuation coefficient. In addition, artifacts due to missing transmission data can cause estimates of the attenuation coefficient for surrounding regions to be inaccurate. For this reason, much effort has be made to develop methods to analyze samples with dense inclusions.

The approach to analyzing samples with dense inclusions is conceptually simple. The desire is to increase the measurement time for the dense regions in order to determine their attenuation coefficient more precisely. However, in practice, the scanning protocol is fixed and there is no incentive on the part of the operator to decrease throughput for samples with dense inclusions, nor is there any way to know *a priori* that opaque regions are present (e.g. sample weight is not necessarily a good indication). A reasonable alternative is to combine measurements of a dense region together to produce a single measurement with improved precision. This is equivalent to increasing scan time and can be accomplished without changing the scanning protocol. By combining measurements,

the resolution in the vicinity of the dense region is reduced. The penalty is an increase in assay bias.

We have developed analytical methods for assaying samples with dense inclusions that minimize bias in the assay (resolution is maximized) while meeting preset constraints on the magnitude of the statistical variation introduced by the transmission mode. These methods have been used over the past three years for TGS analysis and have been shown to function robustly. Algorithms for analyzing samples with dense inclusions are currently considered proprietary and will be published after the successful commercialization of TGS. Without revealing proprietary information, it is possible to demonstrate the performance of the approach.

For example, Figure 5 shows a heterogeneous, 208-l drum phantom that contains a number of dense regions (middle). On the left is a tomograph of the attenuation coefficient obtained using the standard, 30 minute TGS scan. The tomograph on the right was obtained by scanning the sample 5-times longer. Note that the tomograph obtained using the long scan has well-defined inclusions that correspond to the phantom (middle). The standard scan is blurry and not all of the inclusions can be identified. The artifacts introduced in the short scan occur because the variance of portions of the data set exceeded the threshold value. Part of the data set was collapsed and, in doing so, resolution was reduced.

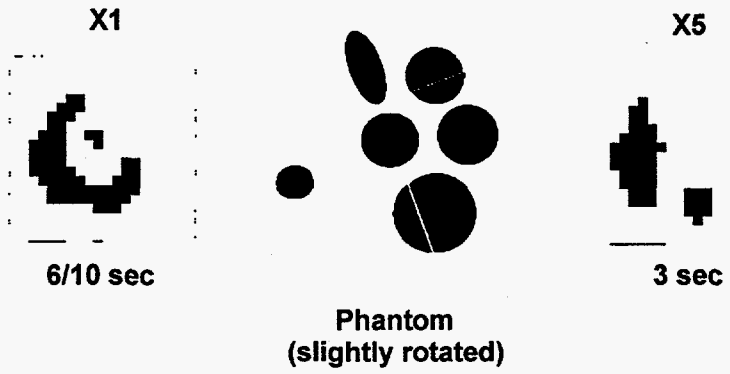

Figure 5. A 208-l drum phantom with dense inclusions and tomographs of the attenuation coefficient obtained for different scan times.

To see how the assay is affected, consider Figure 6. Radioactive material (Pu-239) was placed in one of the inclusions and complete transmission scans of the sample were made for different scan times. A relative measurement time of 1 corresponds to the standard TGS scan. A single 30-minute scan was used to acquire the emission data. As transmission scan time is increased, the number of measurements with acceptable statistical quality increases. Consequently, the number of collapsed measurements (bins) decreases and the accuracy of the assay improves. The precision (or variance) of the assay remains constant. Direct reconstruction of the transmission data, without treating the problem of opacity, resulted in indeterminate results.

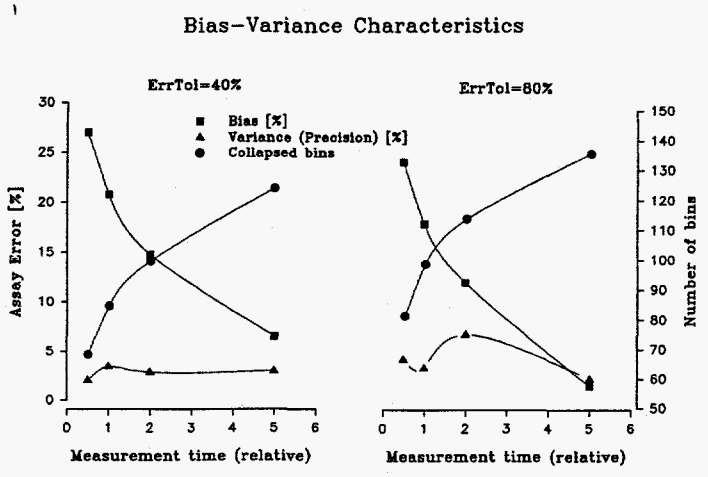

Figure 6. Bias-variance characteristics for a sample with dense inclusions.

All of the methods developed to date for dense-inclusion analysis are based on the projection-domain interpolation algorithm described earlier. The reason is simple. It is easier to operate on the measurements than on the reconstructed attenuation maps. Fitting the energy dependence of the measurements is faster and introduces less variance into the assay than the image-domain approach. When opaque regions are encountered, the measurements can be combined or smoothed to eliminate degenerate cases. Energy correlations in the measurements can be exploited just as easily as in the image. Because the measurements can be processed in blocks, projection-domain interpolation can be applied to large-scale problems.

A practical example of the application of dense-inclusion analysis is the assay of Pu-239 in 208-l drums containing cemented sludge. Cement drums are dense, weighing up to 1000 lbs. Because they can contain large quantities of Am-241, they are often difficult to assay using neutron-based methods. Traditional gamma-ray techniques such as SGS are impractical because the distribution of plutonium is nonuniform. It is possible to assay these drums with TGS. For example, TGS assays of 10 drums containing cemented sludge contaminated with plutonium are compared to declared amounts of Pu-239 in Figure 7. Three of the drums were constructed in the laboratory using Portland cement. The three points correspond to the placement of a standard at three different radial locations in the drum. TGS images of one of the contaminated drums are shown in Figure 8. This drum weighed over 900 lbs. and was found to contain separate distributions of Pu-239 and Am-241. The average bias observed for these drums is 20%. The inventory difference was less than 5%. The case of cement drums, while extreme, illustrates the necessity of dense-inclusion analysis.

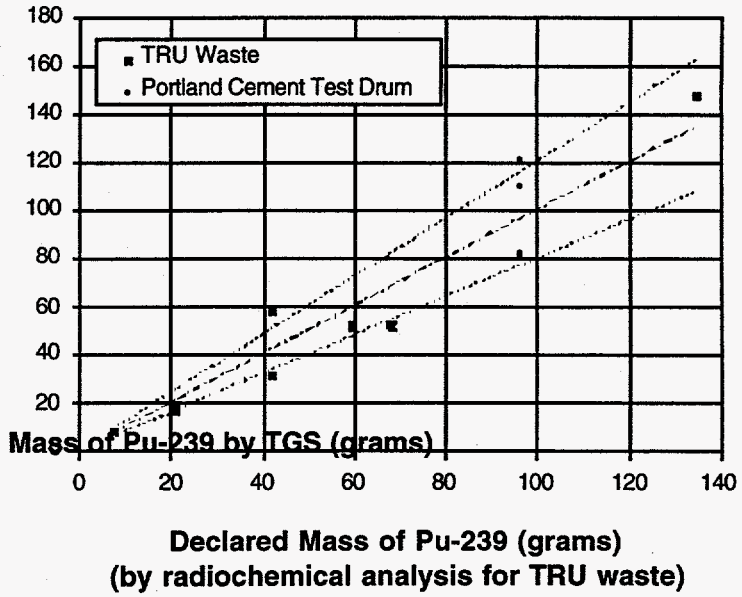

Figure 7. Results of assays of 208-l drums containing cemented sludge.

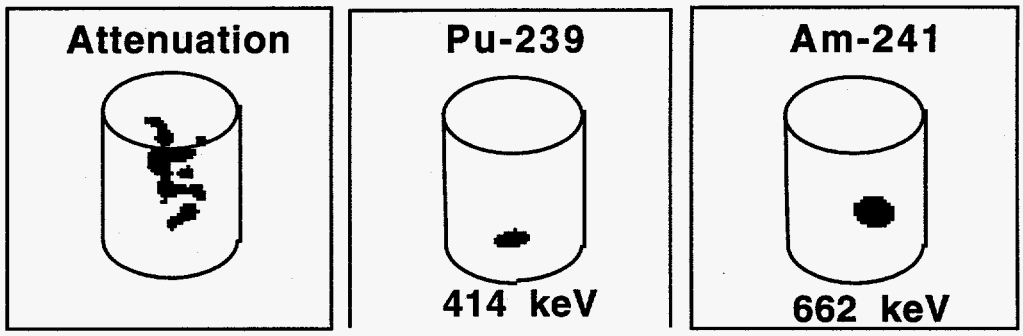

Figure 8. TGS images of a drum containing cemented sludge.

Emission Reconstruction

The objective of the emission analysis is to determine the spatial distribution of selected radioisotopes within the sample, corrected for attenuation by the matrix. To accomplish this, the sample is scanned with the source shutter closed. The emission data set consists of ROI counts ($G_{e,l}$,c_e,$B_{e,l}$) for selected gamma-rays emitted by radionuclides in the sample and ROI counts for a reference gamma-ray emitted by a "live-time" source ($G_{R,l}$,c_R,$B_{R,l}$), where k and l are the energy and measurement indices, respectively. The subscript e was selected to differentiate the emission energies from the transmission measurements. The emission data are corrected for rate-loss using Eq. 1:

$$C_{e,l} = \left(G_{e,l} - c_e B_{e,l}\right) \cdot CF(RL) \qquad \text{Eq. 15}$$

The starting point for the emission analysis is a model that relates the activity or mass of the selected radionuclide to the corrected counts:

$$C(s,\theta,z) = k\iiint_V d^3r\ m(\mathbf{r})\varepsilon_{s,\theta,z}(\mathbf{r})W_{s,\theta,z}(\mathbf{r}) \qquad \text{Eq. 16}$$

where m is the concentration of the isotope (e.g. g/cm^3) at the emission site, $\mathbf{r}$=(x,y,z), ε is the efficiency of the collimated detector, also known as the acceptance function, and W is a weighting function that models the attenuation of the gamma-ray from the interaction site to the detector. The constant k depends on the branching ratio of the gamma-ray, the half-life of the isotope, and counting time. The acceptance function can be measured using a point-source or computed by Monte Carlo for any detector-collimator combination. The attenuation function can be modeled as

$$W_{s,\theta,z}(\mathbf{r}) = \frac{1}{\Omega_r}\int_W d\hat{\Omega}\ \exp\left[-\int_0^{T_{s,\theta,z}(\mathbf{r},\hat{\Omega})} ds\ \mu(\mathbf{r},E)\right] \qquad \text{Eq. 17}$$

where W is the set of all directions to the detector from emission site, Ω_r is the solid angle of the detector, and $T_{s,\theta,z}$ is the distance from the emission site to the detector in the specified direction, $\hat{\Omega}$. The linear attenuation coefficient, $\mu(\mathbf{r},E)$, is determined separately in the transmission analysis.

Following the approach taken to discretize the transmission equations, we represent the concentration as the sum of basis functions:

$$m(\mathbf{r}) = \sum_i m_i B_i(\mathbf{r}) \qquad \text{Eq. 18}$$

Unlike the transmission problem, the sample is represented using finite elements. Finite elements can be used to represent samples of arbitrary shape. In addition, the size and shape of the elements can be varied arbitrarily throughout the sample volume. Compared with other image models, the volume-integral of Eq. 16 is relatively simple to implement.

Substitution of Eq. 18 into Eq. 16 yields the following expression:

$$C(s,\theta,z) = \sum_i m_i a_i(s,\theta,z) \qquad \text{Eq. 19}$$

where

$$a_i(s,\theta,z) = k\iiint_V d^3r\ B_i(\mathbf{r})\varepsilon_{s,\theta,z}(\mathbf{r})W_{s,\theta,z}(\mathbf{r}) \qquad \text{Eq. 20}$$

The discretized emission equations (Eqns. 18-20) provide an accurate model of the measurements that is linear in terms of the coefficients of the basis expression for mass. Consequently, the emission reconstruction algorithm involves solving a linear system:

$$\mathbf{c} = \mathbf{Am} \qquad \text{Eq. 21}$$

where **c** is a column vector of length M whose elements are the data ($c_j = C_{e,j}$), **A** is a matrix with M rows and N columns whose elements are $a_{ij} = a_j(s_i, \theta_i, z_i)$, and **m** is a column vector of length N whose elements are the unknown coefficients of the basis function. For standard TGS problems, the number of unknowns is typically on the order of N=1600 and the number of measurements M=2500. So, the system is over-determined.

Solution of Eq. 21 for **m** is accomplished using maximum likelihood or least squares. The solution is constrained to be positive. For the maximum likelihood problem, an iterative, expectation-maximization algorithm is used. In formulating the maximum-likelihood problem, the statistical structure of the data must be considered. The corrected emission counts are not Poisson variates, and are, in fact, given by the difference of scaled-Poisson variates. Exact treatment of the statistical structure of the data is necessary when small amounts of material are present and the signal-to-noise ratio is large (Prettyman, et al., 1995). Work is currently underway to develop algorithms that function robustly under these conditions.

The principle challenge for emission reconstruction is the assembly of the system matrix **A**. Calculation of the elements of **A** (Eq. 20) is straight-forward, but time-consuming. In low-resolution mode, the detector can see a large portion of the object. The problem cannot be de-coupled into axial layers and the number of nonzero elements in the system matrix is large (Figure 9). Storage of medium-resolution problems with full-precision can be a problem. In addition, because the size of the collimator opening is large, more than one ray must be used to accurately represent attenuation by the sample. A significant portion of the time is spent evaluating Eq. 17.

To enable high-throughput calculations of the system matrix, we have implemented parallel processing techniques for workstation clusters. The calculation of elements of the system matrix can be de-coupled completely. Consequently, the calculation can be broken up into tasks that can be completed on separate processors. The system matrix assembly code is implemented using Parallel Virtual Machine, which runs on Unix and Windows/NT. Load-balancing is accomplished using the "pool-of-tasks" paradigm. We have tested the code on a number of platforms, including 10-node IBM RS-6000 workstation clusters, heterogeneous Unix workstation clusters, and multi-node 300 MHz DEC Alpha clusters. Communication is not limited to the ethernet. For example, the IBM RS-6000 cluster utilized a giga-switch. However, the granularity of the problem can be adjusted so that message passing is not the time-limiting factor. Using a single DEC alpha computer, the assembly of the emission matrix for a low-resolution problem takes less than a minute, which is more than adequate for field applications. We have found that throughput scales with the number of nodes. The assemble time will

decrease significantly when 4-processor Pentium Pro computers with Windows NT become available later this year.

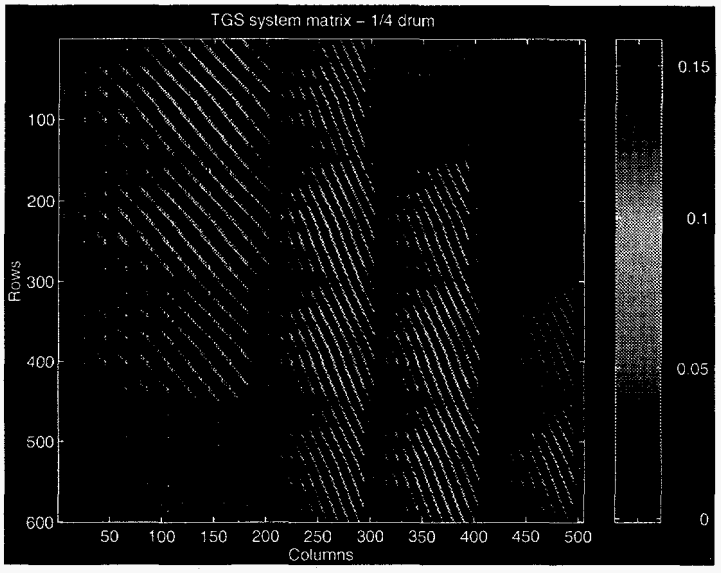

Figure 9. System matrix (**A**) for the emission problem. 70% of the elements are nonzero.

Application of the emission computerized tomography to nondestructive assay is straight-forward. The emission reconstruction problem is solved to determine concentration. The total mass in the sample or in a selected region-of-interest is determined by integrating the concentration over the volume. The calibration constant, k, can be determined using a standard or from first-principles. Algorithms to estimate the uncertainty in the mass have been developed (Prettyman, 1995). Mass estimates obtained for different gamma-ray lines for a single isotope can be combined to improve the precision of the assay or to detect and correct for self-attenuation (Prettyman, Foster, and Estep, 1996).

Summary

We have presented a discussion of the algorithms underlying TGS transmission and emission algorithms. These algorithms have been in use over the past three years for the analysis of data obtained by the prototype and mobile TGS systems. These systems have been used to assay hundreds of samples, including small samples containing plutonium residues and full-sized drums containing transuranic waste. The performance of TGS has been demonstrated with assays of heterogeneous test-drums with a variety of matrix materials, working reference standards, and samples containing residue and waste material known quantities of special nuclear material. A summary of the performance of TGS is presented in Table 2. The accuracy of the results that have been achieved reflect the quality of the underlying analytical methods.

Accuracy for matrix corrections	For heterogeneous samples: • $\rho_A < 30$ g/cm^2 Bias range is $\pm$5% (low density) • $30 < \rho_A < 60$ g/cm^2 Bias range is $\pm$10% (medium density)
Density limitations	For dense, heterogeneous samples (no lumps): • $60 < \rho_A < 120$ g/cm^2 Bias range is $\pm$25% (high density) • Robustness
Inventory difference	The bias in the inventory of SNM determined by TGS should not exceed 5% in the medium density range.
Accuracy for self-attenuation corrections	For low-density samples: • Reliable detection of self-attenuation (e.g. by Pu or U metal) • Detection of saturation conditions (sensitivity-limited) • Bias range is +10%
Precision	• Target quantification limit: 1 g Pu-239 and 5 g U-235 in 1-hr. for medium-density samples (two-pass scan) • Preset scan-time capability

Table 4. Performance of TGS for the assay of heterogeneous material.

References

R. J. Estep, "Assay of Heterogeneous Radioactive Wastes by Low-Resolution Tomographic Gamma Scanning," ANS Transactions 62, 178 (1990).

R. J. Estep and K. Sherwood, "A Prototype Tomographic Gamma Scanner for Assaying 208-Liter Drums," Los Alamos National Laboratory report LA-UR-91-61 (1991).

R. J. Estep, "TGS_FIT: Image Reconstruction Software for Quantitative, Low-Resolution Tomographic Assays," Los Alamos National Laboratory report LA-12497-MS (1993).

R. J. Estep, T. H. Prettyman, and G. A. Sheppard, "Tomographic Gamma Scanning (TGS) to Measure inhomogeneous Nuclear Material Matrices from Future Fuel Cycles," Los Alamos National Laboratory report LA-UR-93-1637 (1993), presented at the Global '93 International Conference and Technology Exhibition on Future Nuclear Systems, September, 1993.

T. H. Prettyman, M. M. Pickrell, and K. L. Coop, "Technology Development for Nondestructive Waste Characterization," Los Alamos National Laboratory report LA-UR-93-1198 (1993).

T. H. Prettyman, R. J. Estep, and G. A. Sheppard, "Development of a Tomographic Instrument for Gamma-Ray Nondestructive Assay," Los Alamos National Laboratory report LA-UR-93-2580, Rev. 1 (1993) presented at the ANS Winter Meeting, November, 1993.

T. H. Prettyman, J. K. Sprinkle, Jr., and G. A. Sheppard, "A Weighted Least-Squares Lump Correction Algorithm for Transmission-Corrected Gamma-Ray Nondestructive Assay," Nucl. Mater. Manage. XXII (Proc. Issue) 682-690 (1993).

R. J. Estep and J. T. Cavender, "The WIN_TGS Software Package for Tomographic Gamma Scanner Systems," Los Alamos National Laboratory report LA-UR-94-2386 (1994), presented at the 35th INMM meeting, July 17-20, 1994.

T. H. Prettyman, J. K. Sprinkle, Jr., and G. A. Sheppard, "Performance of an Advanced Lump Correction Algorithm for Gamma-Ray Assays of Plutonium," Los Alamos National Laboratory report LA-UR-94-2477 (1994), presented at the 35th INMM meeting, July 17-20, 1994.

G. A. Sheppard, T. H. Prettyman, and E. C. Piquette, "Accounting for Segment Correlations in Segmented Gamma-Ray Scans," Los Alamos National Laboratory report LA-UR-94-2561 (1994), presented at the 35th INMM meeting, July 17-20, 1994.

R. J. Estep, T. H. Prettyman, and G. A. Sheppard, "Tomographic Gamma Scanning to Assay Heterogeneous Radioactive Waste," Nucl. Sci. Eng. 118, 145-152 (1994).

T. H. Prettyman, R. A. Cole, R. J. Estep, and G. A. Sheppard, "A Maximum-Likelihood Reconstruction Algorithm for Tomographic Gamma-Ray Nondestructive Assay," Nucl. Inst. Meth. in Phys. Res. A 356 (1995) 470-475.

T. H. Prettyman, "Precision Estimates for Tomographic Nondestructive Assay," Proc. 5th International Conference on Facility Operations-Safeguards Interface, American Nuclear Society, 191-199 (September, 1995).

T. H. Prettyman, S. E. Betts, D. P. Taggart, R. J. Estep, N. J. Nicholas, M. C. Lucas, and R. A. Harlan, "Field Experience with a Mobile Tomographic Gamma Scanner," Proc. 4th Nondestructive Assay and Nondestructive Examination Waste Characterization Conference, 109-137 (October, 1995).

T. H. Prettyman, L. A. Foster, and R. J. Estep, "Detection and Measurement of Gamma-Ray Self-Attenuation in Plutonium Residues," Presented at the Institute of Nuclear Materials Management 37th Annual Meeting, Naples, FL, July 28-31, 1996 (to appear).

T. H. Prettyman, L. A. Foster, "Transmission Computerized Tomography of Dense Objects," Presented at the 3rd Topical Meeting on Industrial Radiation and Radioisotope Measurements and Applications, Raleigh, NC, October 6-9, 1996 (to appear).